ARTICLE

Received 00th January 20xx, Accepted 00th January 20xx

DOI: 10.1039/x0xx00000x

Between carbide and nitride MAX phases: Sol-gel assisted synthesis and characterization of the carbonitride phase $Cr_2GaC_{1-x}N_x$

Niels Kubitza^a, Isabel Huck^a, Hanna Pazniak^b, Curran Kalha^c, David Koch^d, Bo Zhao^d, Pardeep K. Thakur^e, Tien-Lin Lee^e, Aysha A. Riaz^c, Wolfgang Donner^d, Hongbin Zhang^d, Benjamin Moss^f, Ulf Wiedwald^b, Anna Regoutz^c, and *Christina S. Birkel^{a,g}

MAX phases are almost exclusively known as carbides, while nitrides and carbonitrides form a significantly underrepresented subgroup even though they have been shown to possess enhanced properties in comparison to their carbide counterparts. One example is the nitride phase Cr_2GaN which exhibits a spin density wave magnetic state below T = 170 K, while the metallic carbide phase Cr_2GaC follows the MAX phase-typical Pauli-paramagnetic behavior. To investigate the influence on the materials/functional properties of mixing carbon and nitrogen on the X-site, this study aims to synthesize and comprehensively characterize the hitherto unknown carbonitride phase $Cr_2GaC_{1-x}N_x$ and compare it to the parent phases. Due to the challenging synthesis of (carbo)nitrides in general, a sol-gel-assisted approach is applied which was recently developed by our group. This process was further improved by using time-efficient microwave heating, leading to a highly phase pure product. STEM-EDX analyses reveal a C/N ratio of roughly 2:1. Temperature-dependent XRD measurements confirm the literature-known magnetic phase transition of the parent nitride phase Cr_2GaN , while the incorporation of carbon suppresses the latter. Nonetheless, magnetic characterization of the phases reveals that the magnetic behavior can be specifically influenced by changing the composition of the X-site, resulting in an increase of the susceptibility by increasing the nitrogen amount. Overall, these findings further substantiate the big potential in nitrogen-containing MAX phases, which will also serve as starting materials for future doping studies, i.e. on the M- and A-site, and as precursors for novel 2D MXenes.

Introduction

MAX phases are a class of layered ternary metal carbides and nitrides that have attracted particular attention due to their outstanding ability to combine metallic and ceramic properties within one substance class. The discovery of this unique combination of properties can be attributed to Barsoum *et al.* with the synthesis and characterization of Ti₃SiC₂ in 1996.¹ However, the initial preparation of these types of structures reaches back to 1960, when Kudielka *et al.* synthesized titanium and zirconium-based carbosulfides.² Further extensive contributions were made by Jeitschko *et al.* with the

synthesis of the so-called H-phases³⁻⁶ that nowadays are called MAX phases (a term coined by Barsoum et al. in the early 2000s).7 They are summarized with the general chemical formula of $M_{n+1}AX_n$ (n = 1, 2, 3 etc.), where M is an early transition metal, A is a main group element mostly of groups 13 and 14, and X is carbon and/or nitrogen. The crystal structure can be described by edge-shared M_6X octahedra interleaved with layers of A elements, resulting in the space group P63/mmc.8 While the first comprehensive review on MAX phases by Barsoum et al. in 2000 reported roughly 50 MAX phases,7 the current number has increased to more than 340 different compounds, including solid solutions.9 Based on this steadily increasing number it is not surprising that the variety in properties has also become more versatile, such as the discovery of superconducting MAX phases,10-12 their role to serve as precursors for two-dimensional materials, the MXenes, 13 or to exhibit an exceptional and complex magnetic behavior. 14-16 The profound interest in magnetism was sparked by the synthesis of the first magnetic MAX phase (Cr_{0.75}Mn_{0.25})₂GeC in 2013¹⁷ and has become even stronger with the successful preparation of Mn₂GaC thin films, ¹⁸ showing ferromagnetic response up to 230 K and an antiferromagnetic ordering temperature over 500 K.19 Since then, the research on magnetic MAX phases has mainly focused on the synthesis of new manganese doped chromium-based MAX phases,

Corresponding author: Christina S. Birkel

Electronic Supplementary Information (ESI) available: [details of any supplementary information available should be included here]. See DOI: 10.1039/x0xx00000x

^aDepartment of Chemistry, Technische Universität Darmstadt, Germany

^bFaculty of Physics and Center for Nanointegration Duisburg-Essen, University of Duisburg-Essen, Germany

^cDepartment of Chemistry, University College London, London, WC1H 0AJ, UK.

^dInstitute of Materials Science, Technische Universität Darmstadt, 64287 Darmstadt

^dInstitute of Materials Science, Technische Universität Darmstadt, 64287 Darmstadt, Germany

^eDiamond House, Harwell Science and Innovation Campus, Fermi Ave, Didcot, OX11 ODE, UK. ^IDepartment of Chemistry, Molecular Science Research Hub, White City Campus, Imperial College London, London W12 OBZ, UK.

^oSchool of Molecular Sciences, Arizona State University, Tempe AZ-85282, USA. Email: christina.Birkel@asu.edu

with gallium, 16,20,21 germanium, 17,22,23 particularly and aluminum 15,24,25 as the A-element, while new approaches also deal with the incorporation of ferromagnetic elements on the A-site of the MAX phases using chemical replacement techniques.^{26,27} However, most of these reports address solely carbide-based MAX phases, while (carbo)nitride compounds (in total < 30) are significantly underrepresented by a factor of ~10.9 Reasons for these low numbers can be explained by inhibiting aspects during their synthesis, such as the high bonding energy of nitrogen or its gaseous state under normal conditions which aggravates direct nitridation reactions. Thus, the synthesis of nitrogen-rich precursor compounds is required as an additional step in the synthesis chain before the final reaction towards the ternary MAX phase is favorable.^{28,29} It follows, reports on magnetic studies of conventionally synthesized nitride-based MAX phases, not to mention carbonitride phases, are only rare and to the best of our knowledge restricted to the 211 chromium-based MAX phase Cr₂GaN,³⁰ and the recently published V₂GeC_{1-x}N_x system,³¹ although it is known that nitrides often possess an enhanced exchange correlation.32

Liu et al. comprehensively characterized Cr₂GaN using temperaturedependent magnetic, as well as resistivity measurements and found a spin-density-wave transition (SDW) state below $T_N = 170$ K possibly due to Fermi surface nesting.³⁰ Subsequent temperature dependent X-ray diffraction studies by Tong et al. showed an anomalous c/a increase of Cr₂GaN at around 170 K that further substantiated the origin of the occurring SDW state.33 On the contrary, the isostructural carbide pendant Cr₂GaC did not show any anomalous temperature-dependent structural changes and thus no anomalies in the physical properties. $^{\rm 33}$ The magnetism of the pure parent phase without any doping elements is restricted to Pauli paramagnetism.^{30,33} In 2015, further investigations within the Cr₂GaN system were made by Li et al. by doping Cr₂GaN with germanium to induce superconductivity.³⁴ Even though suppression of the SDW state in Cr₂GaN was realized by germanium-doping, no superconducting behavior was observed.³⁴ Instead of doping on the A-site of the MAX phase, producing a solid solution between the carbide and nitride (hence, doping on the X-site) is also expected to slightly change the density of states at the Fermi level (E_F) and thus possibly leading to interesting cooperative phenomena like (anti)ferromagnetism or superconductivity. Therefore, we here report the synthesis and comprehensive characterization of the carbonitride phase Cr₂GaC_{1-x}N_x. The hitherto unknown carbonitride phase was synthesized by a sol-gel assisted solid-state method that has recently been developed by our group in order to circumvent the above stated challenges accompanied with the synthesis of (carbo)nitrides.35 Additionally, microwave heating was used for heating the reaction mixtures and to drastically reduce the reaction time for the synthesis of the new carbonitride and the carbide parent MAX phase. The products were structurally characterized by means of (temperature-dependent) X-ray powder diffraction (XRD), electron microscopy (SEM/TEM), and soft and hard X-ray photoelectron spectroscopy (SXPS/HAXPES). Additionally, functional properties were evaluated by magnetometry, as well as electronic transport and heat capacity measurements. Density functional theory (DFT) calculations support the structural physical characterization of the materials.

Experimental

Step 1-Precursor CrC_{1-x}N_x synthesis:

Following the "urea-glass" method³⁶, 6.0 g (22.5 mmol, 1 eq.) of $CrCl_3 \cdot 6H_2O$ (Alfa Aesar, 99 %) were dissolved in ~8 ml ethanol and heated to 50 °C, before 6.8 g (113.2 mmol, 5 eq.) urea (>99 %, Sigma Aldrich) were added. After 30 minutes of stirring, a highly viscous and greenish gel was obtained, which was then transferred into an alumina crucible and annealed inside a horizontal tube furnace (Carbolite) at 780 °C (3 °C/min heating rate) for five hours under flowing nitrogen. After washing with 3×10 ml of de-ionized (DI) water, a phase pure product was obtained (Figure SI-1, Table SI-1).

Step 2- MAX phase synthesis:

The Cr_2GaC phase was prepared by using exclusively elemental precursors, while nitride and carbonitride precursors, respectively, were used for the synthesis of Cr_2GaN and carbonitride $Cr_2GaC_{1-x}N_x$ (Figure 1).

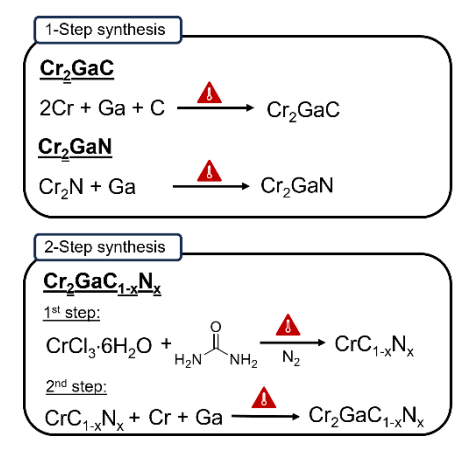


Figure 1: Synthesis scheme for the preparation of the target materials Cr_2GaC , Cr_2GaN , and the new carbonitride $Cr_2GaC_{1:x}N_x$.

All precursor amounts were based on 0.5 g of the desired MAX phase. A detailed summary can be found in the SI (Table SI-2). First, gallium flakes (Alfa Aesar, > 99 %) were cut under atmospheric conditions and subsequently transferred into an argon-filled glovebox. Inside the glovebox, the gallium flakes were loosely mixed with the remaining reactants (chromium, 99 %, Sigma-Aldrich; chromium nitride, Alfa Aesar; graphite, >99 %, Alfa Aesar) according to the reaction equations above and pressed into a dense pellet (\varnothing = 10 mm, 3 t, 5 s). Afterwards, the pellets were transferred into fused silica ampoules and heat treated in the microwave oven (CEM Microwave Technology Ltd.) under flowing argon or vertical tube furnace (Carbolite) under vacuum (Table SI-3). Prior to characterization of the samples, the pellets were finely ground using an agate mortar and stored under atmospheric conditions.

Characterization

X-ray powder diffraction data were obtained using a Stadi P (Stoe & Cie GmbH) with monochromatized Cu-K α_1 radiation (λ = 1.540596 Å) and the Mythen 1K (Dectris) detector in transmission geometry at room temperature. For measurements, small sample amounts were deposited between X-ray amorphous adhesive film (Scotch) on a flat sample holder and rotated orthogonally to the X-ray source. Rietveld

refinements were performed using the program TOPAS (Bruker) and the FullProf-suite³⁷. Temperature-dependent X-ray diffraction was performed on a custom-made setup using transmission geometry and Mo-K α_{1+2} (λ = 0.709320 + 0.713400 Å) radiation. The sample was mixed with NIST SRM 640d silicon powder and glued on a thermally conductive graphite foil. The temperature was controlled using a closed cycle He-cryofurnace.

Ab initio calculations based on density functional theory (DFT) were performed using the Vienna *ab initio* simulation package (VASP), 38,39 which the projector augmented wave implemented. The generalized gradient approximation (GGA) of Perdew–Burke–Ernzerhof was used as the exchange correlation functional. 40 The wave functions were expanded with a 24 \times 24 \times 6 Monkhorst-Pack k-sampling grid and cutoff energy of 500 eV. Calculations for different ratios of N and C were performed within the virtual crystal approximation (VCA) model. 41 The precision of total energy convergence for the self-consistent field (SCF) calculations was 10^{-6} eV. All structures were fully optimized until the maximal Hellmann–Feynman force was less than 10^{-3} eV/Å.

SEM images were taken at the XL30 FEG (Philips) using an acceleration voltage of 20 kV adapted with an APOLLO X-SDD detector (EDAX) for collecting EDX data. The EDX data were evaluated using the software EDAX GENESIS.

Bright-field (BF) high-resolution TEM (HRTEM) and scanning TEM (STEM) images were acquired with a JEOL 2200FS transmission electron microscope at an acceleration voltage of 200 kV using a 2k × 2k GATAN UltraScan1000XP CCD camera. The local chemical composition was determined using EDX in STEM mode with an Oxford windowless 80 mm² SDD X-MaxN 80 TLE detector with 0.21 sr solid angle. HRTEM and EDX data were analyzed using Gatan Micrograph Suite and Oxford's Aztec software, respectively.

SXPS measurements were initially conducted using a laboratorybased Thermo Scientific K-Alpha XPS instrument ($h\nu$ = 1486.7 eV), however, at this photon energy the family of Ga LMM Auger peaks (located between kinetic energies of 790-1100 eV) overlaps with the key N 1s and Cr 2p core levels (Figure SI-3/SI-2). For this reason, synchrotron-based XPS measurements were conducted, where the tunability of the soft X-ray energy enables moving the Auger lines relative to the core levels. Soft and hard X-ray photoelectron spectroscopy (SXPS and HAXPES) measurements were conducted at beamline IO9 (Surface and Interface Structural Analysis) at the Diamond Light Source, UK. SXPS measurements were conducted at a photon energy of 1794.3 eV (1.8 keV) to avoid the overlap of crucial core states with the Ga LMM Auger peaks. This photon energy was achieved by using a 400 lines/mm plane grating monochromator, which provided a total energy resolution of approximately 400 meV (determined by extracting the 16%/84% width of a clean polycrystalline gold foil Fermi edge). HAXPES measurements were conducted at a photon energy of 5926.7 eV (5.9 keV), achieved using a Si(111) double crystal monochromator and a Si(004) post-channelcut crystal, providing a total energy resolution of approximately 300 meV. The end-station at IO9 operates at a base pressure of 3×10⁻¹⁰ mbar and is equipped with a VG Scienta Omicron EW4000 highvoltage electron analyzer with a $\pm 28^{\circ}$ wide acceptance angle.

Samples were mounted on adhesive conductive carbon tape with the X-ray spot for both soft and hard X-rays converging on the same sample position. Survey, key core level (Ga $2p_{3/2}$, Cr 2p, O 1s, N 1s, C 1s), and valence band (VB) spectra were acquired at both photon energies.

Electronic transport, vibrating sample magnetometry (VSM) and specific heat measurements were studied in a PPMS DynaCool system (Quantum Design). For VSM, dried powders (20-30 mg) were weighed and put into polymer capsules. Measurements were taken within the field range of ±9 T at variable temperatures ranging from 3 to 400 K. Resistivity measurements were carried out in four-point in-line geometry at a constant current of 10 mA using a custom-made sample holder and the electrical transport option (ETO). Dense pellets were prepared by placing powder samples into a 12 mm diameter cylindrical mold and applying 7.5-9 tons using a manual hydraulic press. Pressed samples with an average thickness of 0.3 mm (Cr_2GaN) and 0.44 mm ($Cr_2GaC_{1-x}N_x$) were carefully cut into a rectangle (5 mm wide and 10 mm long). Specific heat was measured using the heat capacity option. The Cr₂GaC_{1-x}N_x sample powder (92 mg) was pressed in cylindrical shape with 3 mm diameter by a hydraulic press at 0.5 tons.

Results and discussion

Structural analysis

Rietveld refinements of the X-ray powder diffraction data including the extracted lattice parameters of the targeted Cr₂GaC_{1-x}N_x MAX phase samples are shown in Figure 2 and Table 1. The data of the nitride-based MAX phase were fitted to the structural model of Cr₂GaN,⁴² while the data of the carbide and carbonitride phase were fitted to the structural model of Cr₂GaC.⁴³ As shown in Figure 2, all samples were obtained nearly single-phase with only small amounts of side phases, such as Cr₃GaN (3.3 wt-% in Cr₂GaN; 0.7 wt% in $Cr_2GaC_{1-x}N_x$), $CrGa_4$ (3.9 wt-% in Cr_2GaN ; 1.8 wt-% in Cr_2GaC), and Cr₃Ga (0.3 wt-% in Cr₂GaC). The obtained lattice parameters of both, the carbide Cr₂GaC and nitride Cr₂GaN phase are in good agreement with the values reported in the literature. 42,43 Comparing the c-lattice parameter of the carbonitride phase Cr₂GaC_{1-x}N_x with that of the parent compounds, it is closer to that of the carbide than that of the nitride (which is confirmed by spectroscopy methods, see below). This can also be visualized in the enlarged 2θ region of the (103) and (006) peaks, where the (006) peak of the nitride phase exhibits a noticeable shift compared to the other two phases. On the other hand, the a-lattice parameters of all three phases are too similar to point out significant differences. Overall, a simple estimation of the carbon/nitrogen amount based on XRD and lattice parameter comparison is not feasible and further modeling and investigations by means of XPS and EDX measurements are necessary. This is supported by DFT calculations (Table-SI 4) which reveal that no Vegard behavior is expected when varying the C/N ratio on the X-

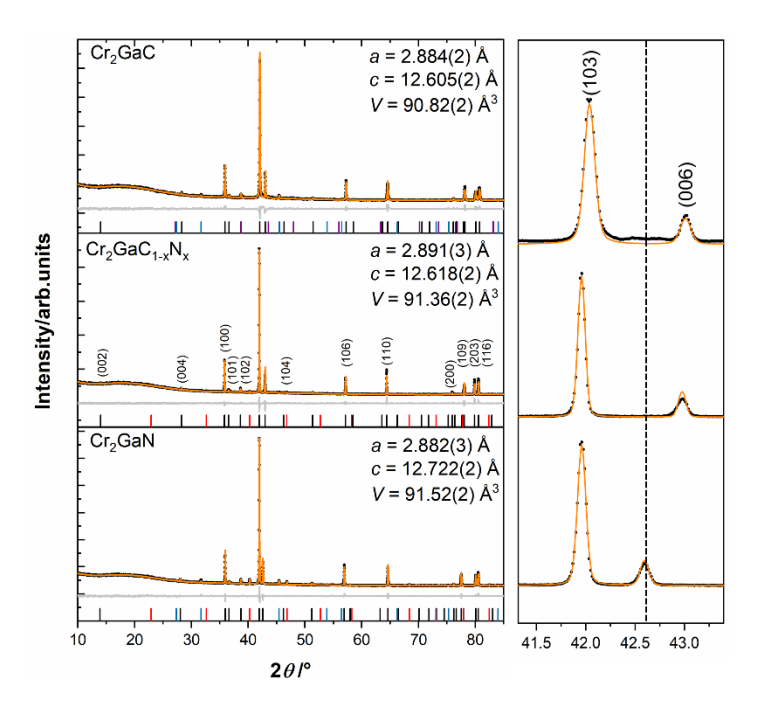


Figure 2: Results of the Rietveld refinements (orange lines) and residuum curves (grey) of the X-ray powder diffraction data (black dots) of Cr_2GaN , Cr_2GaC and $Cr_2GaC_{1.x}N_x$. The refinements were conducted based on structural models of $Cr_2GaN^{42}/Cr_2GaC^{43}$ (black), Cr_3GaN (red), 44 $CrGa_4$ (blue), Cr_3Ga^{46} (purple).

Table 1: Results of the Rietveld refinement of the targeted MAX phase samples.

Phase name	Cr ₂ GaC	$Cr_2GaC_{1-x}N_x$	Cr₂GaN
Space group	P6₃/mmc	P6₃/mmc	P6 ₃ /mmc
Lattice parameters / Å	a = 2.884(2) c = 12.605(2)	<i>a</i> = 2.891(3) <i>c</i> =12.618(2)	a =2.882(3) c =12.722(2)
Cell volume / ų	90.82(2)	91.36(2)	91.52(2)
Background order	15	15	15
R _P	3.74	3.15	3.19
R_{wp}	5.73	5.09	4.55
R _{exp}	2.09	1.82	2.04
GOF	2.74	2.80	2.23

Besides room-temperature X-ray powder diffraction data, temperature dependent (20-300 K) diffraction data were obtained (Figure 2) in order to investigate possible structural anomalous behavior that was initially observed for the nitride phase by Tong et al.33 The latter was attributed to a spin density wave (SDW) transition, shown with an abrupt increase of the c/a lattice parameter ratio at 170 K. Thus, temperature-dependent diffraction data can be used as an indicator for an SDW state in the carbonitride phase. Analogous to the room temperature diffraction data, Rietveld refinements were conducted to extract the temperature-dependent lattice parameters of the samples. As shown in Figure 3(a), the α lattice parameter decreases monotonically with decreasing temperature for all three compounds. The c-lattice parameter, however, decreases for both, the Cr₂GaN and Cr₂GaC phase, whereas the c-lattice parameter of the nitride phase anomalously increases below 140 K (Figure 3 (b)). In general, these results are in good agreement with the reported data of Tong $et~al.^{33}$, however, the anomalous c-lattice parameter change appears at ~30 K lower temperatures than what was reported previously. For the carbonitride phase $Cr_2GaC_{1-x}N_x$, no anomalous structural change was observed, rather the behavior was similar to the carbide phase Cr_2GaC . Since no anomalous change in the structure is obtained, the SDW state is suppressed in the carbonitride but can be reproduced for the nitride.

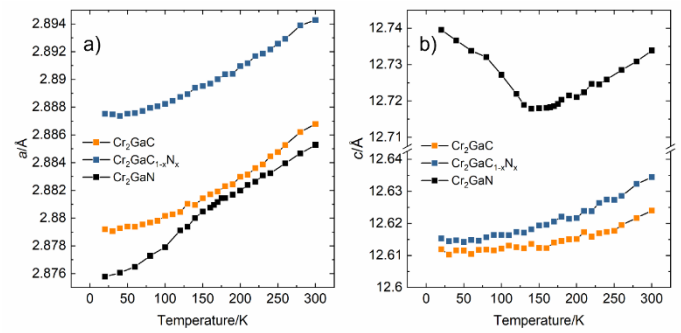


Figure 3: Temperature-dependent (20-300 K) lattice parameters of Cr_2GaN , Cr_2GaC and $Cr_2GaC_{1:x}N_x$. (a) shows the T-dependency of the a-lattice parameter, while (b) shows the T-dependency of the c-lattice parameter.

For further characterization of the synthesized MAX phases, electron microscopy studies were conducted. However, due to the literature known parent phases, the following data are restricted to the new carbonitride $\text{Cr}_2\text{GaC}_{1-x}\text{N}_x$. SEM micrographs reveal its morphology, which can be described as a mixture of typical MAX phase layered structures (Figure 4(c)), as well as particles, whose surfaces are covered with smaller drop-like substructures (Figure 4(a)), typical for sol-gel based syntheses. 47,48 On the other hand, TEM micrographs show a mixture of elongated and spherical particles (Figure 4(b)), whereas the corresponding HRTEM micrograph (Figure 4(d)) reveals the high crystallinity of the sample which is supported by the Fast Fourier Transformation (FFT) shown in the inset of Figure 4(d).

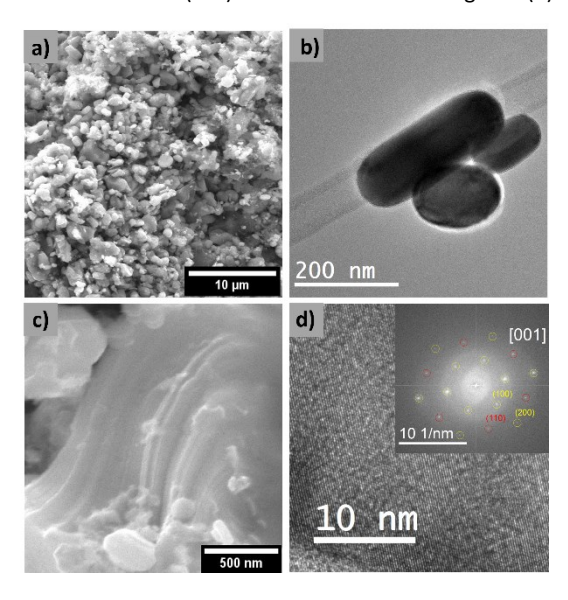


Figure 4: SEM electron micrographs (a,c) showing the morphology of the carbonitride MAX phase, while (HR)TEM micrographs show the particle shape (b) and the well-ordered MAX phase typical structure (d), supported by the FFT (d, inset). The zone axis

is [001] and 6 spots for the (100) and (200) planes are marked by yellow circles while (110) spots are indicated red.

Additionally, the FFT of the HRTEM image was used to calculate the averaged d-spacings from the distances of all spots to the origin. This allows to determine the zone axis to [001] and to assign Miller indices hkl to the obtained spacings of d_{100} = 2.45 Å and d_{110} = 1.37 Å. These results are in reasonable agreement with the d-spacings derived by the XRD data (d_{100} = 2.504 Å and d_{110} = 1.446 Å) by considering a larger error bar of the FFT evaluation.

Due to the calculated and measured non-linear evolution of the lattice parameters of the carbonitride phase based on the amount of the X-element, XRD cannot deliver the stoichiometry. Instead, STEM-EDX mappings were conducted to estimate the C/N ratio in the MAX phase. In Figure 5, a representative elemental map of a particle of the investigated phase is shown. All expected atomic signals of the MAX phase are detected, however, the carbon and nitrogen signals are slightly inhomogeneously distributed. This can most likely be explained by amorphous carbon residues as a result of the sol-gelbased synthesis approach as well as by a varying thickness or selfshadowing effects in the direction of the EDX detector. Nonetheless, both elemental signals are present over the whole particle. Averaged over the whole area, the elemental ratio of the phase can be quantified as Cr₅₁Ga₂₄C₁₇N₈, leading to an estimated overall C/N ratio of ~ 2:1. The detected oxygen signal can be explained by surface oxidation of the particles originating from the sol-gel based synthesis procedure and treatment under ambient conditions.

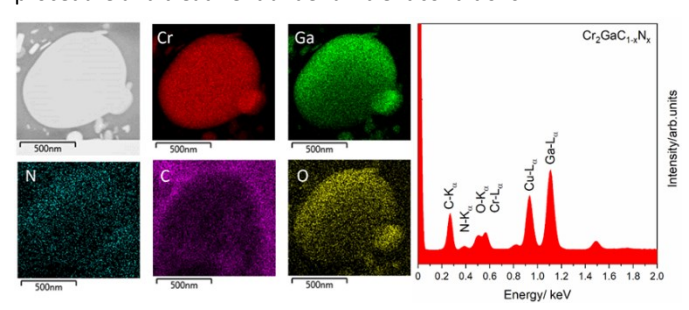


Figure 5: STEM-EDX mappings showing the distribution of the elements in the carbonitride MAX phase, including a representative EDX spectrum for determining the C/N ratio.

To complement the XRD data and infer the chemical state of the material, SXPS and HAXPES data on the three samples were collected $% \left(1\right) =\left(1\right) \left(1\right)$ at beamline IO9 at photon energies of 1.8 and 5.9 keV, respectively. Changing the photon energy ($h\nu$) between the soft and hard X-ray regimes during the measurements allows for control over the probing depth, a strategy exploited in the authors' previous work. $^{\rm 35}$ The maximum relativistic inelastic mean free path (IMFP) of photoelectrons exiting the Cr₂GaC sample surface can be calculated using the TPP-2M predictive formula implemented in the QUASES software package.⁴⁹ Cr₂GaC does not exist in the QUASES database. Therefore, a new material was created (assuming a bulk density of 7.09 g/cm³,⁵⁰ atomic mass of 185.73 u, 19 valence electrons, and metallic behaviour (no band gap). The maximum relativistic IMFP of photoelectrons from Cr₂GaC at a photon energy of 1.8 and 5.9 keV is calculated to be 2.7 and 7.2 nm, respectively, equating to an estimated probing depth of 8.1 and 21.6 nm (assuming 3×IMFP =

probing depth). The survey spectra collected at both photon energies (Figure SI-4) display strong signals from the expected elements (Ga, Cr, O, C and N). Minor signals from chlorine (≈200 and 270 eV) and sodium (≈1071 eV) are also observed in the spectra of the Cr₂GaN and Cr₂GaC samples, respectively. SXPS shows that using a photon energy of 1.8 keV ensured that the Ga LMM Auger peaks did not overlap with the key core levels. Figure 5 displays the Ga $2p_{3/2}$, Cr 2p, N 1s, and C 1s core level spectra as a function of photon energy. The O 1s and valence band spectra collected with SXPS and HAXPES can be found in Figure SI-5. The collected valence band spectra (see Figure SI-5(b/d)) show that for all samples a distinct Fermi edge is observed, with it being more distinct when measured with HAXPES, indicating metallic character. The presence of a Fermi edge enables the binding energy (BE) scale of all core level spectra to be referenced to the intrinsic Fermi energy (E_F) of the respective samples. Due to the nature of the samples and the lack of charge compensation mechanisms at the synchrotron, partial charging occurred during the measurements, leading to different levels of distortion on the higher BE side of the spectra. This was also experienced in the authors' previous work on the V-Ga-C/N MAX phases.35 Nevertheless, the spectra still provide valuable insight into the chemical states of the samples, but quantification of the chemical states cannot be performed. The Ga $2p_{3/2}$ spectra displayed in Figure 6 (a) show that when measured with SXPS, a main intensity peak at 1118.6 eV is observed, commensurate with an oxygen-terminated gallium (Ga-O) chemical environment.35 This peak is the most intense for the mixed carbonitride phase. A subtle asymmetry is also observed on the lower BE side of this peak when measured with soft X-rays, which is attributed to the Ga-C/N environment.35 Figure 6 (e) shows that with increasing photon energy (and therefore increasing probing depth), the intensity of this Ga-C/N environment (BE = 1116.5 eV) significantly increases relative to the Ga-O peak intensity. This suggests that the surface of these samples is oxidized, whereas the bulk is carbonitride-rich. An additional peak and/or broadening is observed on the higher BE side of the Ga-O peak with both soft and hard X-rays (labelled with an asterisk, *). The assignment of this spectral feature is difficult to confirm owing to the partial charging of the spectra and, therefore, cannot be discussed further. Similar charging effects are found in the other core level spectra. Additionally, the XRD data showed side phases (albeit at low concentration), and the resulting chemical environments will contribute to the core level spectra. The Cr 2p spectra in Figure 6 (b) and (f) display similar attributes to the Ga $2p_{3/2}$ core level in that a low BE peak at 574.3 eV (Cr $2p_{3/2}$) is observed, and its signal intensity is enhanced with HAXPES. This peak is attributed to the primary Cr- $\mbox{C/N}$ environment, $\mbox{}^{51,52}$ and given the depth sensitivity of this peak when measured with HAXPES, it again suggests that the carbonitride is situated toward the bulk of the sample. The higher BE features observed in the Cr 2p spectra are associated with an oxygenterminated Cr environment (Cr-O). 51,52 As for the Ga $2p_{3/2}$ core level, the side phases observed in XRD will also contribute to the Cr 2p spectra. The N 1s and C 1s spectra displayed in Figures 6 (c) and (g), and (d) and (h), respectively, provide direct confirmation that the desired carbonitride phases were obtained for the three samples.

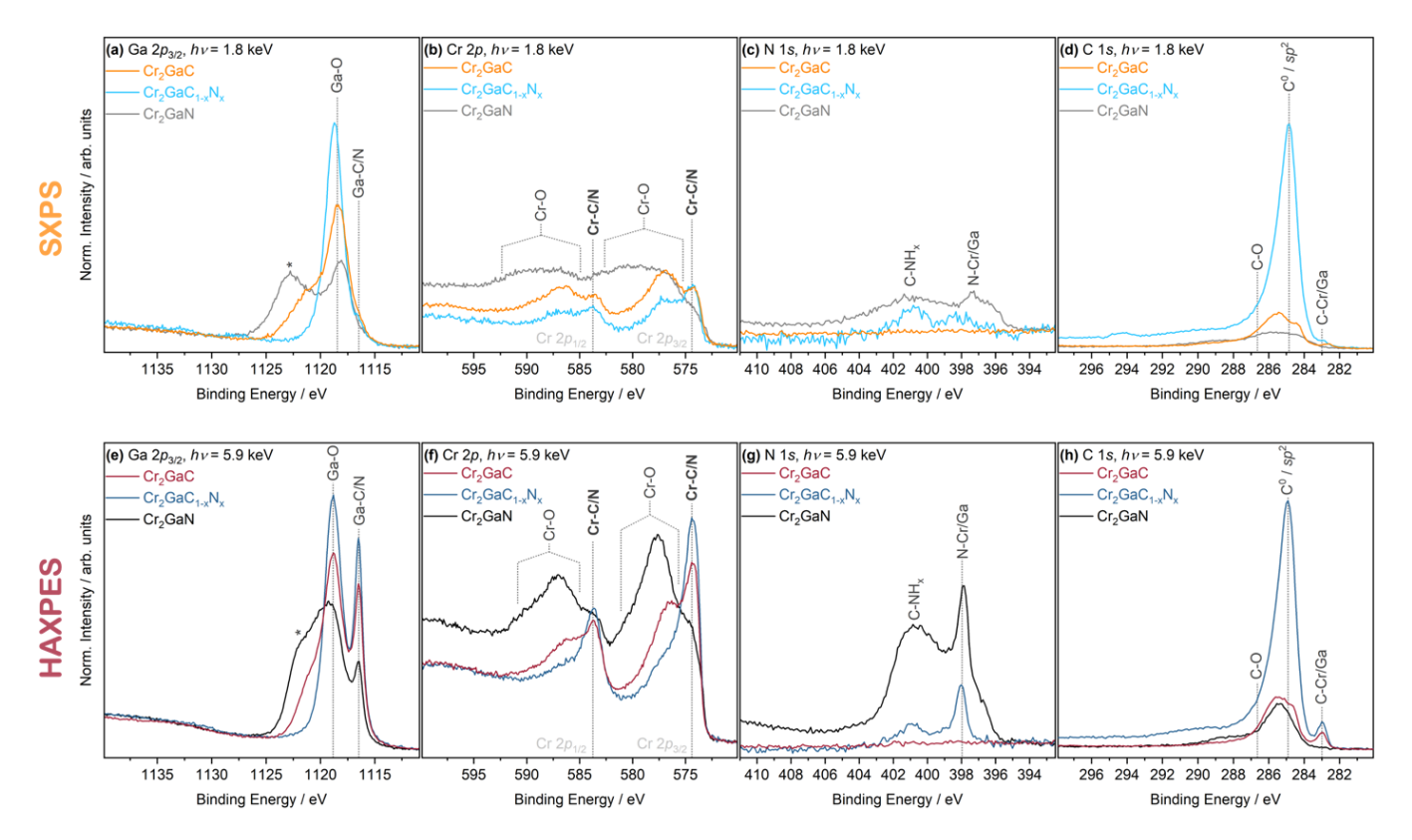


Figure 6: Labelled SXPS ($h\nu = 1.8$ keV) and HAXPES ($h\nu = 5.9$ keV) core level spectra of the carbonitride samples, including (a/e) Ga $2p_{3/2}$, (b/f) Cr 2p, (c/g) N 1s, and (d/h) C 1s. The top row (a-d) contains the spectra collected with SXPS, and the bottom row (e-h) contains the equivalent spectra collected with HAXPES. The spectra are normalized to the total spectral Ga $2p_{3/2}$ area, and the linear y-axis is set so that each spectrum has a similar signal-to-noise ratio.

The lower BE peak at approx. 283.0 eV in the C 1s spectra is commensurate with a metal-carbide environment (C-Cr/Ga), 35,53 and is only observed in the Cr_2GaC and $Cr_2GaC_{1-x}N_x$ samples. In the N 1s spectra, the lower BE peak at 397.8-398.0 eV is commensurate with a metal-nitride environment (N-Cr/Ga), 35,54 and is only observed in the expected sample. In both the C/N 1s spectra, the carbonitride environments are more easily observed with HAXPES, which indicates that the bulk of these samples is carbonitride-rich, whereas the surface is oxidized. Furthermore, in both the N and C 1s spectra, the intensity of metal carbide/nitride peaks increase with respect to the total Ga $2p_{3/2}$ in the expected trend. Higher BE features are also observed in both C/N 1s spectra, with the C 1s spectra dominated by graphitic sp² carbon, adventitious carbon (C⁰) and carbon-oxygen species, whereas in the N 1s spectra a broader peak is observed at +2.8 eV from the N-Ga/Cr and is most likely attributed to organic nitrogen species (e.g. C-NH_x).⁵⁵ Lastly, it is noted that with respect to the total Ga $2p_{3/2}$ peak intensity, the mixed carbonitride sample has the most intense C 1s signal, in both soft and hard XP spectra. Figures 6 (d and h) show that the total normalized C 1s signal intensity of the mixed carbonitride sample is roughly three times that of the signal measured on the nitride and carbide samples. The reason for the dominant C signal in the carbonitride sample can be related to the synthesis procedure. A sol-gel synthesis approach was employed, using urea as a gelling agent. During the heat treatment step, urea will be converted into amorphous carbon that is also retained in the product phase. The SEM images (Figure 4) verify that free amorphous

carbon particles are indeed present at the surface and throughout the sample. This also explains why the dominate peak within the C 1s spectra for the mixed carbonitride sample displays an asymmetric profile, commensurate with a graphitic sp^2 -like environment. To conclude, the variance in probing depth achieved with the combination of SXPS and HAXPES confirms that all samples are carbo/nitride-rich in the bulk with an oxide overlayer on the surface. Furthermore, we obtain the expected carbo/nitride chemical environments for each sample as well as showing the influence of the synthesis procedure on the final products.

Magnetic analysis

The magnetic properties of the three different MAX phase samples may give additional insights into the influence of the carbon amount on the materials properties of the MAX phases. Figure 7 (a) shows the temperature-dependent magnetization curves of all three materials in a small field of $B=10\,\mathrm{mT}$ and a temperature range of 3-400 K. Practically over the whole temperature range, both carbon-containing phases show an almost temperature-independent behavior, indicating MAX phase-typical Pauli paramagnetism. For This is in accordance with the DFT calculations (Table SI-4), showing that no magnetic ordering in the ground state is expected up to a nitrogen incorporation of at least 50 at-%. However, it must be noted that the magnetic state of the carbonitride $Cr_2GaC_{1-x}N_x$ switches to diamagnetic response at around 7 K, pointing towards superconducting characteristics. In contrast, Figure 7 (a) shows that

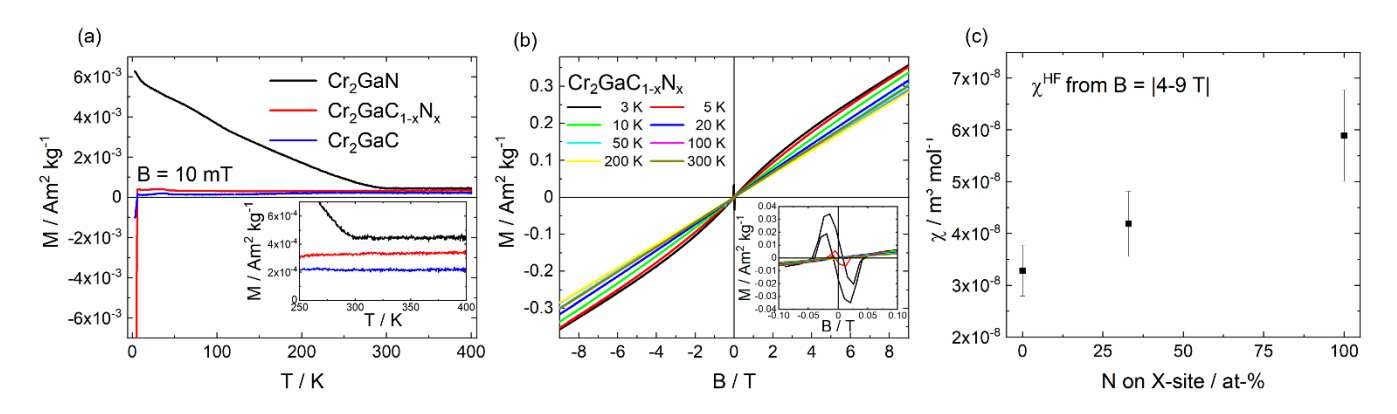


Figure 7: a) Temperature-dependent magnetization curves of $Cr_2GaC_{1.x}N_x$, and Cr_2GaN in a field of B = 10 mT and a temperature range of 3-400 K. b) Field-dependent magnetization of $Cr_2GaC_{1.x}N_x$ at various temperatures between 3-300 K. c) Magnetic susceptibility from the field-dependent magnetization data of $Cr_2GaC_{1.x}N_x$, and Cr_2GaN at 300 K. The susceptibility is extracted from linear fitting of the signal in the interval |B| = 4-9 T. The nitrogen amount of the carbonitride is based on the EDX measurements presented in Figure 4.

the pure nitride phase Cr2GaN exhibits a strong temperaturedependent magnetization in the temperature range of 3-300 K, since the magnetization values varying of more than one order of magnitude, which can be attributed to the SDW state in the system.³⁰ At 300 K however, this changes towards Pauli paramagnetism, analogous to Cr_2GaC and $Cr_2GaC_{1-x}N_x$. Figure 7 (b) shows the isothermal field-dependent magnetization curves of the new carbonitride phase Cr₂GaC_{1-x}N_x. From 20-300 K, all curves are strictly linear at high fields and the absolute magnetization at 300 K at 9 T (0.30 Am^2kg^{-1}) only differs by ~15 % from the absolute magnetization at 3 K (0.35 Am²kg⁻¹), which confirms the Pauli paramagnetic behavior as discussed above. Supporting the temperaturedependent measurements (Figure 7 (a)), the hysteresis curves exhibit at 3 K and 5 K a superconducting response as shown in the inset of Figure 7 (b). Besides, both curves show a slight non-linearity at higher fields that can be explained by small amounts of Langevinparamagnetic impurities which are not visible in the XRD data. Figure 7 (c) presents the magnetic susceptibility values extracted from the linear fitting of the field-dependent magnetization curves at 300 K in

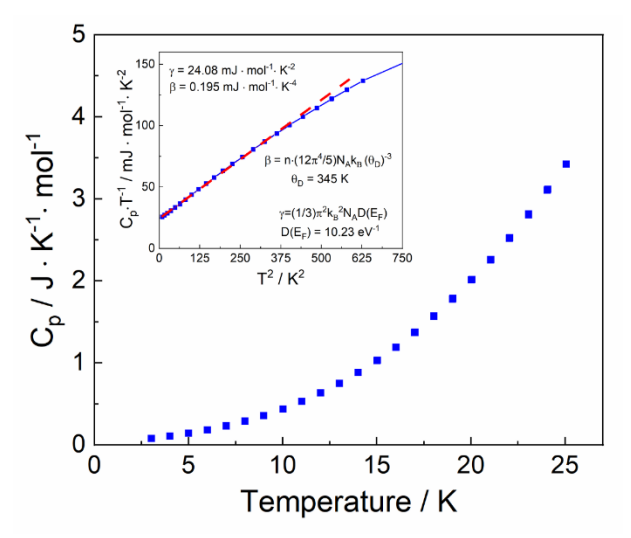


Figure 8: Low-temperature specific heat measurements including the inset of $C_p T^{\,\text{-}1}$ plotted against $T^2.$

the interval of |B| = 4-9 T. Supporting the temperature-dependent magnetization data in Figure 7 (a), the susceptibility significantly increases by increasing the nitrogen amount on the X-site of the MAX phase by the factor of almost two from carbide to nitride. Based on the determined nitrogen amount of the carbonitride phase (Figure 5), these results suggest a linear correlation of the susceptibility and the amount of nitrogen in the MAX phase. To further evaluate the possible superconducting behavior of the carbonitride phase below 7 K, specific heat, as well as electronic transport measurements were conducted. While the latter should show a zero net resistivity below the critical temperature T_{c} , the specific heat should show an abrupt change at T_c.⁵⁷ As shown in Figure 8, no anomalous behavior of the specific heat in the low temperature range can be observed, which disproves the possibility of a new carbonitride bulk superconductor. Rather, the superconducting signal in the magnetic analysis data arises from minor fractions of side phases. Nonetheless, the lowtemperature specific heat can be used to calculate the density of states at the Fermi level ($D(E_F)$ if plotted as C_pT^{-1} against T^2 (Figure 8 inset), as described elsewhere. 33 By performing a linear regression of the specific heat data,³³ the $D(E_F)$ of the carbonitride results in 10.23 states per eV, which is around 20 % higher than the calculated value for a nitrogen amount of 30 % presented in Table SI-4. The deviation can be most likely explained by the presence of the amorphous carbon in the material system, also influencing the Debye temperature θ_D , as well as the physical simplifications related to the applied Sommerfeld model. Analogous to the specific heat measurements, electronic transport measurements (Figure SI-6) do not show any superconducting behavior of the carbonitride phase at the proposed critical temperature $T_c = 7$ K derived from the magnetic measurements. Only the typical metallic behavior for MAX phases is observed since the resistivity steadily decreases upon cooling with a remaining resistivity of 29 $\mu\Omega$ m at 4 K. On the other hand, the pure nitride phase exhibits the literature reported anomalous behavior which can be assigned to the spin-density wave transition, however with 117 K, again at lower temperatures.30 By applying a magnetic field of B = 1 T, the transport properties of the nitride phase are slightly influenced resulting in a small difference of the residual resisitivity RRR (ρ (300 K)/ ρ (4 K)) of ~ 3 %. In general, the lower RRR

values compared to literature values,³³ can be explained due to differences in the pellet preparation process. Overall the absence of bulk superconducting properties in both, transport and specific heat measurements, can be assigned to small amounts of side phases (e.g., Ga-N compounds⁵⁸) which could not be identified in the XRD data.

Conclusions

In this study, we present the synthesis and characterization of Cr₂GaN, Cr₂GaC, and the hitherto unknown carbonitride Cr₂GaC_{1-x}N_x phase. The latter was synthesized applying the sol-gel assisted ureaglass method that was recently developed by our group. Additionally, the reaction time of the final MAX phase formation was drastically reduced due to the use of microwave heating. The carbonitride character was confirmed by means of X-ray powder diffraction data and SXPS/HAXPES measurements, while STEM-EDX measurements revealed the carbon/nitrogen ratio to be 2:1, resulting in a sum formula of $Cr_2GaC_{0.67}N_{0.33}$. Temperature-dependent measurements confirm the literature-reported anomalies in the lattice parameter evolution of the pure nitride Cr₂GaN, that are referred to a spin density wave state (SDW) in the system. On the other hand, the carbonitride and carbide do not show any anomalies, leading to a suppression of the SDW state by the incorporation of carbon into the MAX phase lattice. To further analyze the functional properties of the materials, magnetic, heat capacity as well as resistivity measurements were performed. Magnetic analysis revealed Pauli paramagnetic behavior of the carbon-based phases, while the pure nitride exhibits a strong temperature-dependent magnetization due to the SDW at T < 300 K. Furthermore, the susceptibility of the materials is dependent on the nitrogen amount on the X-site of the MAX phase and is increasing with nitrogen content. Field-dependent magnetization data suggest a superconducting behavior of the carbonitride below T = 7 K, which was disproven by heat capacity and transport measurements and thus ascribed to minor fractions of impurities. Overall, this study substantiates the recently developed sol-gel-assisted method as a valuable option to synthesize new carbonitride MAX phases that exhibit materials properties deviating from their parent phases. It is therefore an elegant tool to manipulate the functional properties of these layered solids, while providing the synthetic base for targeted materials design of MAX phases and beyond.

Author Contributions

The manuscript was written through contributions of all authors. All authors have given approval to the final version of the manuscript.

Conflicts of interest

There are no conflicts to declare.

Acknowledgements

C.K. and A.A.R. acknowledge support from the Department of Chemistry, UCL. We acknowledge Diamond Light Source for time on Beamline I09 under Proposal No. NT29451. The authors would like to thank Dave McCue, I09 beamline technician, for his support of the experiments.

Funding Sources

This work has been supported by the Deutsche Forschungsgemeinschaft (DFG, German Research Foundation) within CRC/TRR 270, projects B03, B02, B04 and A05, (Project-ID 405553726).

References

- M. W. Barsoum and T. El-Raghy, J. Am. Ceram. Soc., 1996,
 79. 1953–1956.
- 2 H. Kudielka and H. Rohde, *Zeitschrift für Krist.*, 1960, **114**, 447–456.
- 3 W. Jeitschko, H. Nowotny and F. Benesovsky, Monatshefte für Chemie, 1964, 95, 156–157.
- 4 W. Jeitschko, H. Nowotny and F. Benesovsky, *Monatshefte für Chemie*, 1963, **94**, 672–676.
- W. Jeitschko, H. Nowotny and F. Benesovsky, *Monatshefte für Chemie*, 1964, **95**, 178–179.
- 6 W. Jeitschko, H. Nowotny and F. Benesovsky, *Monatshefte für Chemie*, 1963, **94**, 844–850.
- 7 M. W. Barsoum, Prog. Solid State Chem., 2000, 28, 201–281.
- 8 M. Sokol, V. Natu, S. Kota and M. W. Barsoum, *Trends Chem.*, 2019, **1**, 210–223.
- 9 M. Dahlqvist, M. W. Barsoum and J. Rosen, *Mater. Today*, 2023, **72**, 1-24.
- A. D. Bortolozo, O. H. Sant'Anna, C. A. M. dos Santos and A.
 J. S. Machado, Solid State Commun., 2007, 144, 419–421.
- A. D. Bortolozo, O. H. Sant'Anna, C. A. M. Dos Santos and A.
 J. S. MacHado, *Mater. Sci. 2012 302*, 2012, 30, 92–97.
- 12 A. D. Bortolozo, O. H. Sant'Anna, M. S. da Luz, C. A. M. dos Santos, A. S. Pereira, K. S. Trentin and A. J. S. Machado, *Solid State Commun.*, 2006, **139**, 57–59.
- M. Naguib, O. Mashtalir, J. Carle, V. Presser, J. Lu, L.
 Hultman, Y. Gogotsi and M. W. Barsoum, ACS Nano, 2012,
 6, 1322–1331.
- A. S. I. and M. D. and J. Rosen, A. S. Ingason, M. Dahlqvist, J. Rosén, A. S. Ingason, M. Dahlqvist, J. Rosén and M. Max, J. Phys. Condens. Matter, 2016, 28, 433003.
- C. M. Hamm, J. D. Bocarsly, G. Seward, U. I. Kramm and C.
 S. Birkel, *J. Mater. Chem. C*, 2017, 5, 5700–5708.
- J. P. Siebert, S. Mallett, M. Juelsholt, H. Pazniak, U. Wiedwald, K. Page De, C. S. Birkel, K. Page and C. S. Birkel, Mater. Chem. Front., 2021, 5, 6082–6091.
- 17 A. S. Ingason, A. Mockute, M. Dahlqvist, F. Magnus, S.

- Olafsson, U. B. Arnalds, B. Alling, I. A. Abrikosov, B. Hjörvarsson, P. O. Å. Persson and J. Rosen, *Phys. Rev. Lett.*, 2013, **110**, 195502.
- A. S. Ingason, A. Petruhins, M. Dahlqvist, F. Magnus, A. Mockute, B. Alling, L. Hultman, I. A. Abrikosov, P. O. Å. Persson and J. Rosen, *Mater. Res. Innov.*, 2014, 2.2, 89–93.
- I. P. Novoselova, A. Petruhins, U. Wiedwald, Á. S. Ingason,
 T. Hase, F. Magnus, V. Kapaklis, J. Palisaitis, M. Spasova, M.
 Farle, J. Rosen and R. Salikhov, *Sci. Rep.*, 2018, 8, 2637.
- S. Lin, P. Tong, B. S. Wang, Y. N. Huang, W. J. Lu, D. F. Shao,
 B. C. Zhao, W. H. Song and Y. P. Sun, J. Appl. Phys., 2013,
 113, 53502.
- 21 M. Yan, C. Li, Y. Zou and M. Yang, *J. Wuhan Univ. Technol. Sci. Ed. 2020 352*, 2020, **35**, 363–367.
- 22 Z. Liu, T. Waki, Y. Tabata and H. Nakamura, *Phys. Rev. B Condens. Matter Mater. Phys.*, 2014, **89**, 054435.
- T. H. Scabarozi, S. Benjamin, B. Adamson, J. Applegate, J.
 Roche, E. Pfeiffer, C. Steinmetz, C. Lunk, M. W. Barsoum, J.
 D. Hettinger and S. E. Lofland, Scr. Mater., 2012, 66, 85–88.
- 24 K. Sobolev, M. Gorshenkov, P. Manfrinetti, D. Peddis, A. Pazniak and V. Rodionova, *Ceram. Int.*, 2021, 47, 21069–21076.
- 25 K. Sobolev, H. Pazniak, M. Farle, V. Rodionova and U. Wiedwald, *J. Mater. Chem. C*, 2021, **9**, 16516–16522.
- Y. Li, J. Liang, H. Ding, J. Lu, X. Mu, P. Yan, X. Zhang, K. Chen, M. Li, P. O. Å. Persson, L. Hultman, P. Eklund, S. Du, H. Yang, Z. Chai and Q. Huang, *Appl. Phys. Rev.*, 2021, 8, 31418.
- 27 H. Ding, Y. Li, M. Li, K. Chen, K. Liang, G. Chen, J. Lu, J. Palisaitis, P. O. Å. Persson, P. Eklund, L. Hultman, S. Du, Z. Chai, Y. Gogotsi and Q. Huang, *Science* (80), 2023, 379, 1130–1135.
- 28 A. L. Greenaway, C. L. Melamed, M. B. Tellekamp, R. Woods-Robinson, E. S. Toberer, J. R. Neilson and A. C. Tamboli, *Annu. Rev. Mater. Res.*, 2020, **51**, 1–28.
- 29 N. Kubitza, C. Büchner, J. Sinclair, R. Snyder and C. S. Birkel, *Chempluschem*, 2023, **88**, e202300214.
- Z. Liu, T. Waki, Y. Tabata, K. Yuge, H. Nakamura and I.
 Watanabe, *Phys. Rev. B Condens. Matter Mater. Phys.*, 2013, 88, 1–7.
- N. Kubitza, B. Beckmann, S. Jankovic, K. Skokov, A. A. Riaz, C. Schlueter, A. Regoutz, O. Gutfleisch and C. S. Birkel, *Chem. Mater.* 2024, **36**, 1375-1384.
- 32 J. M. D. Coey and P. A. I. Smith, *J. Magn. Magn. Mater.*, 1999, **200**, 405–424.
- 33 H. Tong, S. Lin, Y. Huang, P. Tong, W. Song and Y. Sun, *Intermetallics*, 2019, **105**, 39–43.
- 34 Y. Li, J. Liu, W. Liu, X. Zhu and H. H. Wen, *Philos. Mag.*, 2015, **95**, 2831–2837.
- N. Kubitza, A. Reitz, A.-M. Zieschang, H. Pazniak, B. Albert, C. Kalha, C. Schlueter, A. Regoutz, U. Wiedwald and C. S. Birkel, *Inorg. Chem.*, 2022, 61, 10634–10641.
- C. Giordano and M. Antonietti, *Nano Today*, 2011, **6**, 366–380.
- J. Rodríguez-Carvajal, Phys. B Condens. Matter, 1993, 192,
 55–69.

- G. Kresse and J. Furthmüller, *Phys. Rev. B*, 1996, **54**, 11169–11186.
- 39 G. Kresse and D. Joubert, Phys. Rev. B, 1999, 59, 1758– 1775
- J. P. Perdew, K. Burke and M. Ernzerhof, *Phys. Rev. Lett.*,
 1996, 77, 3865–3868.
- 41 L. Bellaiche and D. Vanderbilt, *Phys. Rev. B*, 2000, **61**, 7877–7882.
- 42 O. Beckmann, H. Boller, H. Nowotny and F. Benesovsky, Monatshefte für Chemie, 1969, 100, 1465–1470.
- J. Etzkorn, M. Ade, D. Kotzott, M. Kleczek and H. Hillebrecht, J. Solid State Chem., 2009, 182, 995–1002.
- 44 M. Nardin, G. Lorthioir, M. Barberon, R. Madar, M. E. Fruchart and R. Fruchart, Comptes Rendus Hebd. des Seances des Sci. Ser. C, Sci. Chim., 1972, 274, 2168–2171.
- 45 H.-G. Meissner and K. Schubert, *Zeitschrift für Met.*, 1965, **56**, 523–530.
- Materials Data on Cr3Ga by Materials Project (Dataset) |
 DOE Data Explorer,
 https://www.osti.gov/dataexplorer/biblio/dataset/118869
 6, (accessed 17 December 2021).
- J. P. Siebert, L. Bischoff, M. Lepple, A. Zintler, L. Molina-Luna, U. Wiedwald and C. S. Birkel, *J. Mater. Chem. C*, 2019, **7**, 6034–6040.
- 48 J. P. Siebert, K. Patarakun and C. S. Birkel, *Inorg. Chem.*, 2022, **61**, 1603–1610.
- 49 H. Shinotsuka, S. Tanuma, C. J. Powell and D. R. Penn, Surf. Interface Anal., 2015, 47, 871–888.
- 50 M. Project, Materials Data on Cr2GaC.
- 51 M. Detroye, F. Reniers, C. Buess-Herman and J. Vereecken, *Appl. Surf. Sci.*, 1999, **144–145**, 78–82.
- 52 M. H. Tran, A. M. Malik, M. Dürrschnabel, A. Regoutz, P. Thakur, T.-L. Lee, D. Perera, L. Molina-Luna, K. Albe and J. Rohrer, *Dalt. Trans.*, 2020, **49**, 12215–12221.
- A. Picone, A. Lodesani, M. Capra, A. Brambilla, F. Bottegoni, M. Jugovac, A. K. Kundu, P. M. Sheverdyaeva and P. Moras, Appl. Surf. Sci., 2022, 599, 153926.
- 54 I. Bertóti, *Surf. Coatings Technol.*, 2002, **151–152**, 194–203.
- 55 K. Artyushkova, J. Vac. Sci. Technol. A, 2020, **38**, 31002.
- N. Kubitza, R. Xie, I. Tarasov, C. Shen, H. Zhang, U. Wiedwald and C. S. Birkel, *Chem. Mater.*, 2023, **35**, 4427–4434.
- W. Nolting, Phasenübergänge BT-Grundkurs Theoretische Physik 6: Statistische Physik, Springer Berlin Heidelberg, Berlin, Heidelberg, 2014, pp. 279–415.
- N. E. Alekseevskii, G. V Samsonov and O. I. Shulishova, *Zh. Eksperim. i Teor. Fiz.*, 1963, **44**.